

Combined effect of electrode gap and radio frequency on power deposition and film growth kinetics in SiH₄/H₂ discharges

E. Amanatides, D. Mataras^{a)} and D. E. Rapakoulias

Department of Chemical Engineering, Plasma Technology Laboratory, University of Patras, P.O. Box 1407, 26500 Patras, Greece

(Received 30 May 2001; accepted 1 October 2001)

The combined effect of the variation of the interelectrode gap (1.3–2.5 cm) and radio frequency (13.56–50 MHz) on the properties of highly diluted silane in hydrogen discharges used for the deposition of microcrystalline silicon thin films is presented. The investigation included electrical and optical discharge measurements as well as the *in situ* determination of the film growth rate. In the lower frequencies regime, the increase of the interelectrode gap for the same applied voltage results in higher current flows and higher total power dissipation. On the other hand, at 50 MHz the variation of the interelectrode space has only a slight effect on the total power dissipation, due to the low excitation voltage. However, at all frequencies, the increase of the interelectrode space results in a drop of the power dissipation per discharge volume. This is related to the less effective energy transfer to the electrons that is due to the enhancement of the bulk relative to the sheath ohmic heating. The variation of the relative importance of the electron heating modes is reflected in the discharge radical production efficiency and the film growth rate. © 2002 American Vacuum Society. [DOI: 10.1116/1.1421599]

I. INTRODUCTION

Capacitive radio-frequency (rf) discharges are widely used for the deposition of device quality hydrogenated amorphous (*a*-Si:H) and microcrystalline (μ c-Si:H) silicon thin films for microelectronics.^{1,2} The main macroscopic discharge parameters in the deposition of either *a*-Si:H or μ c-Si:H are the rf power, the rf frequency, the discharge geometry, the nature of the feed gas or the gas mixture, and the total gas pressure. The variation of these parameters can significantly alter the discharge properties by affecting the charged particle kinetics, the gas phase chemistry, and the plasma–surface interaction. Thus, significant effort is required for determination of the optimum deposition conditions, while in most cases the synergetic effect of the different combinations of these discharge parameters has to also be considered in order to extract unambiguous results.

Among the above-mentioned parameters, an increase of the plasma excitation frequency from 13.56 MHz to very high frequency has been found to have a beneficial effect on the film deposition rate³ without significantly affecting the film properties.⁴ This has led to a number of theoretical and experimental studies dealing with the effects of frequency on the plasma structure,⁵ the ion and electron kinetics,⁶ the electron energy distribution function (EEDF),⁷ the power dissipation,⁸ and the production of radicals through electron–molecule collisions.⁹

In addition, the changes of the discharge geometry resulting from the modification of the interelectrode gap have also been the subject of many studies dealing with plasma physics,^{10,11} gas phase chemistry,^{12,13} film growth rate, and properties.^{14–18} More precisely, Godyak *et al.*¹⁰ and Kimura *et al.*¹¹ have reported the EEDF dependence on the gas

pressure–interelectrode gap product *Pd*. In both studies, a transition of the EEDF from a bi-Maxwellian to Maxwellian and to Druyvesteyn type distribution with the increase of *Pd* has been reported, and this transition has been attributed to the change of the electron heating mechanism from the stochastic to the ohmic heating mode. The change of the EEDF with the variation of the basic geometric characteristics of the discharge has also been identified by investigating primary electron–molecule collision processes with different electron energy requirements.¹² In this study, the increase of the interelectrode gap has been found to give a relative enhancement of the low energy processes against high energy ones. Finally, the effect of the variation of the interelectrode space on the deposition rate of *a*-Si:H films as well as on their optoelectronic properties has also been addressed.^{14–18} Although some of the results presented in these studies are controversial, in all these cases interelectrode gap has been identified as an effective external control parameter for optimization of the deposition rate, suppression of particle formation, and improvement of the film properties. However, all these studies were carried out at the conventional frequency of 13.56 MHz and deal only with the deposition of *a*-Si:H thin films.

The work presented here aims at studying the effect of interelectrode gap on the deposition process of μ c-Si:H from highly diluted SiH₄ in H₂ discharges operated at frequencies higher than 13.56 MHz. The basic purpose of the work was to determine the interelectrode gap that optimizes the deposition rate of μ c-Si:H for a specific set of discharge conditions at each frequency in the range from 13.56 to 50 MHz. In this sense, special attention has been given in revealing perturbations in the microscopic discharge parameters that could affect the deposition rate. More precisely, the alteration of the power dissipated in the discharge due to the

^{a)}Author to whom correspondence should be addressed; electronic mail: dim@chemeng.upatras.gr

modification of the interelectrode distance was accurately measured¹⁹ and an effort was made to relate these changes to the relative importance of the bulk/sheath ohmic and stochastic electron heating mechanisms. The changes in the relative importance of these mechanisms were additionally associated with the production of radicals through spatially resolved optical emission spectroscopic measurements. The alteration of the power actually consumed in the discharge and the production of radicals were finally correlated to the film growth rate and discussed in terms of the role of different film precursors.

II. EXPERIMENT

Film deposition studies have been performed in a capacitively coupled ultrahigh vacuum (UHV) parallel plate reactor, with a base vacuum of 10^{-9} mbar. The reactor is equipped with a load lock system for transportation of the substrates and with four quartz windows suitable for spectroscopic observations. The grounded (deposition) electrode (90 mm in diameter) is mounted on an UHV linear motion feedthrough, allowing variation of the interelectrode space. In the present study the distance between the two electrodes has been varied between 1.3 and 2.5 cm. In all cases the 2% SiH_4 in H_2 gas mixture has been delivered in the reactor through a showerhead array of holes in the powered electrode, at a total pressure of 0.5 Torr. Pressure and flow rate are independently adjusted by a downstream throttle valve controller and an upstream mass flow controller, respectively. The films were deposited on Corning 7059 glass substrates, heated at a temperature of 250 °C. The deposition rate was measured *in situ* using laser reflectance interferometry.

The power actually consumed in the discharge and the discharge impedance was determined by using Fourier transform voltage and current analysis. The voltage and current wave forms were measured on the powered electrode lead, using a high impedance 1:100 attenuation voltage probe and a 0.1 Ω transfer impedance rf current probe. The exact method used for the measurement of the power consumed in 13.56 MHz discharges and its extension to include higher frequencies were presented elsewhere.^{8,19} In addition, the setup used for recording spatially resolved emission intensities of SiH ($A^2\Delta \rightarrow X^2\Pi$) have been described in detail elsewhere.²⁰

All the measurements reported here were performed under dust free conditions, as controlled by a laser light scattering technique.²¹

III. RESULTS AND DISCUSSION

A. Power dissipation

The dependence of the total power and the power per discharge volume consumed in 0.5 Torr, 2% SiH_4 in H_2 discharges, on the interelectrode distance is presented in Figs. 1(a) and 1(b), respectively. Namely, the power consumed in the discharge has been measured for electrode gaps ranging from 1.3 to 2.5 cm, for 13.56, 30, and 50 MHz discharges. At each frequency, the peak-to-peak voltage V_{pp} was kept con-

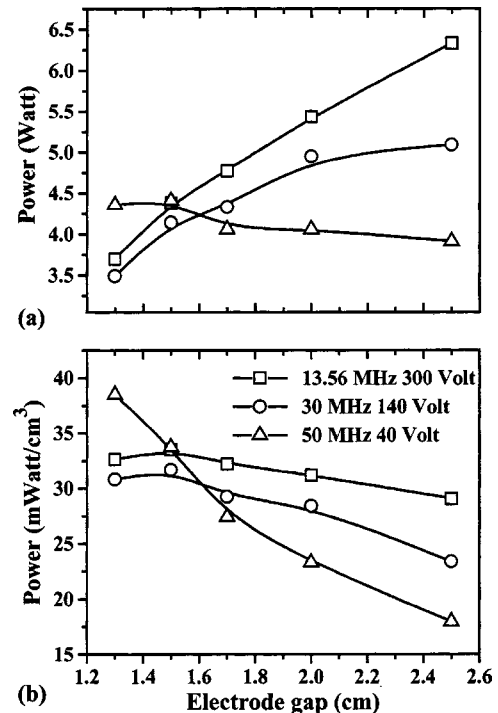


FIG. 1. Variation (a) of the total power dissipation and (b) of the power per discharge volume as a function of the electrode gap for 2% SiH_4 in H_2 discharges and frequencies of 13.56, 30, and 50 MHz.

stant, i.e., 300, 140, and 40 V for 13.56, 30, and 50 MHz, respectively. This gives almost constant power consumption for an interelectrode distance of 1.5 cm independent of frequency. The drop of the voltage required for operating at the same power level independent of frequency has been also reported in previous studies.^{8,22,23} However as shown in Fig. 1, this will also depend strongly on the choice of the electrode gap. In the case of 13.56 and 30 MHz the increase of the interelectrode space is followed by a continuous increase of the total power dissipated in the discharge, whereas at 50 MHz the increase of the interelectrode space has almost no effect on the total power [Fig. 1(a)].

On the other hand, the increase of the electrode gap leads to a drop of the power per volume for all frequencies, which is much more pronounced for the 50 MHz case [Fig. 1(b)]. The estimation of the power per volume is based on the calculation of the discharge volume as a cylinder having as bases the electrode surfaces and height the interelectrode distance. This simple approach is expected to underestimate the discharge volume, since in the case of asymmetrical discharges the reactor walls play an important role in the definition of the grounded area.^{24,25} However, this effect will be more important as the electrode gap increases and the distance between the electrodes becomes comparable to the distance of the electrodes from the reactor walls. Thus, the underestimation of the discharge volume will not affect the trend presented in Fig. 1(b), i.e., the observed drop would be further enhanced by an increase of the discharge volume with the electrode gap.

Figure 2 shows the discharge current and the impedance

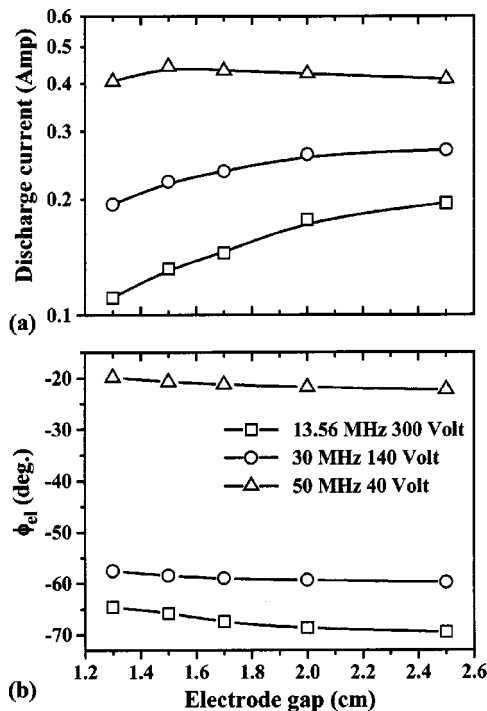


FIG. 2. (a) Total discharge current and (b) phase of the discharge impedance ϕ_{el} as a function of the electrode gap at the conditions of Fig. 1.

phase used for the calculation of the power consumption. The increase of frequency results to higher current flows independent of the interelectrode distance [Fig. 2(a)] due to the higher plasma density.^{5,8} It is worth noting that according to the analytical simulation of Ref. 8 the electron density increases significantly with frequency (13.56 MHz $\sim 4 \times 10^{-8} \text{ cm}^{-3}$, 30 MHz $\sim 7 \times 10^{-8} \text{ cm}^{-3}$, 50 MHz $\sim 3 \times 10^{-9} \text{ cm}^{-3}$). In addition, in the case of 13.56 and 30 MHz, the increase of the interelectrode space results in an increase of the discharge current that is responsible for the higher total power consumption.²⁶ On the contrary, the increase of the electrode gap has no effect on the current flow at 50 MHz, explaining the almost constant total power dissipation at this frequency [Fig. 1(a)].

Although, the increase of the discharge current can fairly well explain the dependence of the total power on the electrode gap, it cannot be simply related to the drop of the power per volume, which indicates a less effective power coupling in the discharge. In this direction the discharge impedance and more precisely the discharge character that is presented in Fig. 2(b) in terms of the discharge impedance phase ϕ_{el} , can be used as a measure of the power deposition effectiveness.^{19,27} It is observed that the increase of frequency results in less negative values of the impedance phase, whereas the increase of the interelectrode gap leads to a shift from a more resistive to a more capacitive regime (i.e., impedance phases from 0° to -90°). The significant decrease of the impedance phase with increasing frequency has been addressed in a previous work of this group⁸ and has been attributed to the rise of inductive behavior in the bulk, as the ratio of excitation frequency ω to the electron-

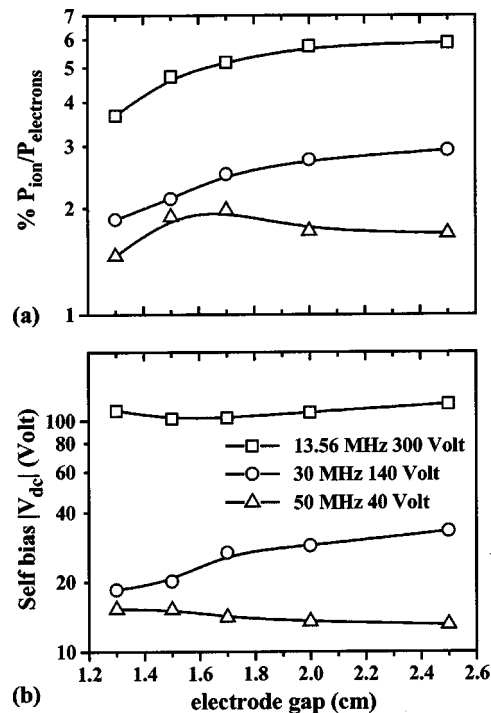


FIG. 3. (a) % fraction of ion relative to electron power and (b) variation of the self-bias potential as a function of the interelectrode gap at the frequencies of 13.56, 30, and 50 MHz.

molecule momentum transfer collision frequency ν_m increases.

The reasons leading to the observed shift toward more capacitive discharges with increasing electrode gap have must lie in changes in the power dissipated by electrons and ions. This is attempted in Fig. 3(a), which presents the fraction of the ion power to the electron power as a function of the interelectrode space. The estimation of electron/ion power is performed by applying the analysis of previous work of this group⁸ to the present results. This analysis is based on the assessment of the mass transport of charged particles in the sheaths and in the bulk, using the electrical parameters of the discharge (current, voltage, impedance) together with an estimation of the spatial distribution of the gas ionization rate, for the calculation of the main microscopic discharge parameters. The power consumed for ion acceleration results from the ion flux toward surfaces and the voltage drop in the sheaths. Moreover, the total power dissipated by electrons is calculated using the ohmic part of the discharge impedance, excluding the resistance that is due to ion power losses.

One can observe that the increase of frequency is associated with a drop of the ion power relative to the electron power, independent of the electrode gap. This is due to the lower excitation voltage used at higher frequencies leading to lower voltage drops in the sheaths. On the contrary, the increase of the electrode gap for the 13.56 and 30 MHz discharges is followed by an enhancement of the ion power, while at 50 MHz the relative power dissipation to ions and electrons remains almost unaffected.

The enhancement of the ion power in the lower frequencies is determined by the changes of the rf sheath voltage. Namely, the increase of the interelectrode gap results in a higher voltage drop in the sheath of the powered electrode due to the change of the self-bias potential V_{dc} . As shown in Fig. 3(b), V_{dc} is enhanced at higher gaps due to an increase in the contribution of the chamber walls to the total grounded surface.^{25,28} More precisely, V_{dc} increases by $\sim 15\%$ as the interelectrode distance increases from 1.5 to 2.5 cm at 13.56 MHz, whereas at 30 MHz this increase is much more pronounced ($\sim 40\%$).

In contrast to what is observed at lower frequencies, at 50 MHz the increase of the electrode gap leads to a slight drop in V_{dc} , indicating that in this frequency the variation of the interelectrode space cannot modify the discharge contact with the reactor walls. This is a result of the very low rf voltage used, which leads to a restriction of the discharge in the area between the two electrodes. Furthermore, the flux of electrons toward the reactor walls is not favored at this frequency because the time required for electrons to escape plasma (cathodic phase and sheath expansion) is higher than the field reversal time. Hence, before electrons have the possibility of escaping from the plasma region, the sheath of the powered electrode starts to collapse (anodic phase and sheath contraction), again allowing the diffusive flux of electrons toward the powered electrode.⁵ These two parameters (i.e., low excitation voltage and electron trapping in the interelectrode space) determine the almost constant values of V_{dc} with increasing electrode gap and consequently the almost constant fraction of ion to electron power.

Thus, the low fraction of ion relative to electron power ($<7\%$ at all frequencies), as well as its increase with the electrode gap, cannot explain the observed drop of the power per volume. Therefore, the reasons for this drop have to be related to the influence of interelectrode space on the power consumed for electron heating.

The basic electron acceleration mechanisms in rf discharges are stochastic and ohmic heating modes.²⁹ The stochastic heating mode has been studied either theoretically^{29,30} or experimentally^{10,11} and was found to be the main electron heating mechanism for values of the product of the total pressure to the electrode gap Pd that are less than 0.6 Torr cm and this is lower than the Pd values used in this study. In all the other conditions, stochastic heating can be neglected and the main mechanism of electron acceleration is ohmic heating. This mechanism is strongly related to the interaction of electrons with the rf field and can be distinguished in bulk and sheath Joule heating modes.³¹ This distinction is necessary because the mechanism is much more effective in the high field sheath regions compared to the low field bulk, despite the much lower electron density in these regions. In this sense, an estimation of the relative importance of the bulk to the sheath ohmic heating mechanism would be useful under the present conditions for understanding the less effective energy coupling at higher electrode gaps. This can be achieved by applying the relation proposed

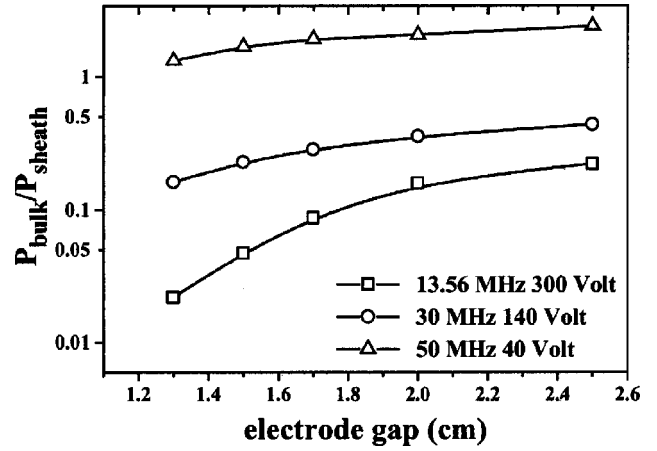


FIG. 4. Effect of the variation of the interelectrode gap on the relative importance of the bulk and the sheath electron collisional heating at the frequencies of 13.56, 30, and 50 MHz.

by Godyak and Lieberman²⁹ for the calculation of the power consumed for electron heating in the bulk:

$$P_b = \int_0^{d_b} \frac{J_{TOT}^2}{2} \left(\frac{m_e v_m(x)}{e^2 n_e(x)} \right) dx \quad (1)$$

and the formula proposed by Lieberman³² and Misium *et al.*³³ for the calculation of electron heating in the sheaths:

$$P_s = \frac{J_{TOT}^2}{2} \left(\frac{m_e v_m}{e^2 n_s} \right) [0.43(0.6V_s/T_e)^{1/2} + 1.16 + 2.4(T_e/(0.6V_s))^{1/2}] s. \quad (2)$$

In Eqs. (1) and (2), $n_e(x)$ and n_s are the electron density in the bulk and in the bulk/sheath boundary, respectively, v_m the momentum transfer electron–molecule collision frequency, J_{TOT} the discharge current density, m_e , e the mass and the charge of electron, V_s the sheath voltage, and T_e the electron temperature in the bulk/sheath interface. In addition, d_b and s are the bulk and the sheath length, respectively. Assuming that the value of v_m remains constant either in the sheaths or in the bulk ($v_m \sim 8 \times 10^9 \text{ Torr}^{-1} \text{ s}^{-1}$ for 3% SiH₄ in H₂ discharges and for electron energies above³⁴ 1 eV), Eqs. (1) and (2) can be combined in order to express the relative importance of the bulk to the sheath ohmic heating as

$$\frac{P_b}{P_s} = \frac{n_s d_b}{[0.43(0.6V_s/T_e)^{1/2} + 1.16 + 2.4(T_e/(0.6V_s))^{1/2}] \bar{n}_e s}, \quad (3)$$

where \bar{n}_e is the spatial average electron density in the bulk plasma.

Thus, Fig. 4 presents the variation of the ratio P_b/P_s as a function of the electrode gap, using the values obtained from the analysis of Ref. 8 and for frequencies of 13.56, 30, and 50 MHz. In the two lower frequencies the increase of the electrode gap results in an enhancement of the bulk relative to the sheath electron heating, however sheath ohmic heating still dominates ($P_b/P_s < 1$) over the entire range of inter-

electrode gaps examined here. The observed increase is due mainly to the increase of the bulk length, whereas the sheath length is not affected by the change of the interelectrode distance, as it will be shown in Sec. IIIB. The other ratios (n_s/n_e and V_s/T_e) involved in Eq. (3), remain unaffected by the variation of the electrode gap. In addition, one can observe in Fig. 3 that the relative importance of the bulk heating increases with frequency. Indeed at 50 MHz the two mechanisms have almost equal importance independent of the electrode gap.

Therefore, the drop of the power per discharge volume that has been presented in Fig. 1(b) can be attributed to the enhancement of the rate of energy transfer to electrons in the bulk compared to the energy transfer in the sheaths. Thus, the increase of the bulk relative to the sheath lengths can lead to an increase of the total power consumption but not to more effective power dissipation. In contrast to the case of the high gaps and/or the high frequencies, in low interelectrode spaces electrons, wherever they are produced in the discharge, will have the chance to interact with the high field oscillating sheaths. Electrons that interact with a high field, attribute the energy gained very fast in high energy inelastic collisions with molecules (excitation, dissociation, ionization), leading to a more effective rate of energy transfer and to higher power dissipation per discharge volume.

B. Radicals production and film growth rate

The change of the total power and the total power per volume caused by the variation of the interelectrode gap under constant voltage operation, are certainly affecting the production of radicals through electron–molecule collisions. The effect of the electrode gap on the high-energy electron impact processes and also on the discharge structure has been investigated using spatially resolved optical emission spectroscopic measurements of the SiH ($A^2\Delta$) radical. Thus, Figs. 5(a) and 5(b) show the spatial emission profiles of this radical at 50 and 30 MHz, respectively, and for electrode gaps ranging from 1.3 to 2.5 cm. The spatial resolution for recording the emission profiles presented here is 0.05 cm. The main difference between the two frequencies is the position of the maximum of emission intensity that in the higher frequency is displaced toward the rf electrode. The change of the electrode gap for the same frequency does not affect the position of the intensity maximum, indicating a constant sheath length independent of the gap as mentioned above. In general the emission intensity is localized close to the bulk/sheath interface, independent of the electrode gap or the frequency, while at very small electrode gaps the emission profiles have an almost triangular shape. This is due mainly to the interaction of the powered and the grounded sheath electron heating mechanisms that finally lead to a maximum rate of production of excited radicals at the center of the discharge. The increase of the electrode gap ($d > 1.7$ cm) is followed by a distinction of the two heating sources that is reflected in the appearance of the less pronounced emission intensity peak close to the grounded electrode.

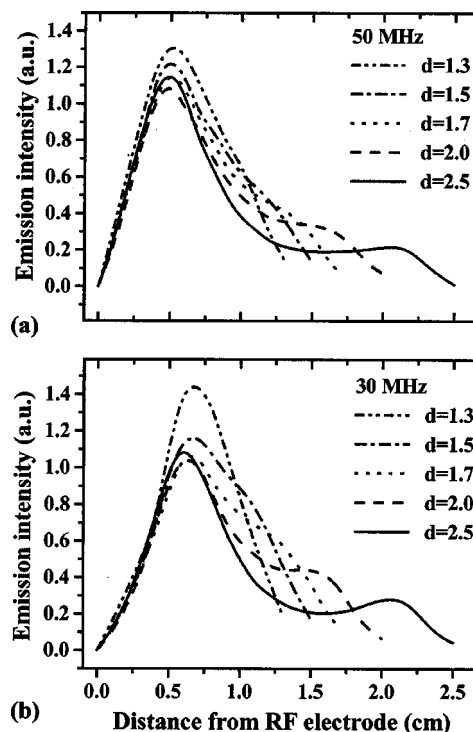


FIG. 5. Spatial distribution of the SiH ($A^2\Delta$) emission intensity at five different electrode gaps at: (a) 50 and (b) 30 MHz.

Another difference that can be observed by comparing the spatial profiles at 30 and 50 MHz lies in the different shape of the emission intensity increase, from the powered electrode to the maximum of intensity. Thus, at 30 MHz the increase of the emission intensity from the powered electrode to the position of the intensity maximum is typically characteristic of electron heating during the expansion of the powered sheath. During the cathodic phase, electrons are pushed away from the momentary cathode by the strong electric field and can consequently contribute to high-energy inelastic processes like the one observed here. On the other hand, at 50 MHz the distribution of emission intensity from the powered electrode to the maximum rate of production increases almost linearly. This is because the sheath contraction and expansion are much less pronounced at 50 MHz than at 30 MHz. Very recently, Yan *et al.*³⁵ using a particle in cell/Monte Carlo simulation have investigated the effect of frequency (13.56 and 65 MHz) on the spatiotemporal profiles of electron heating mechanisms for electropositive and electronegative gases. According to their results, in the high frequency case the sheath expansion is much less pronounced due to the lower operating voltage, while electron heating is much more localized either in space or in time. In the same study, it has been predicted that in the high frequency case, energetic electrons will penetrate shorter distances in the bulk compared to the low frequency case, due to the retardation of electrons from a strongly out of phase bulk field. Both these predictions can explain the fact that in the 50 MHz profiles [Fig. 5(a)] the expansion of the sheath is less pronounced and the profiles are narrower and less expanded toward the grounded electrode compared to 30 MHz.

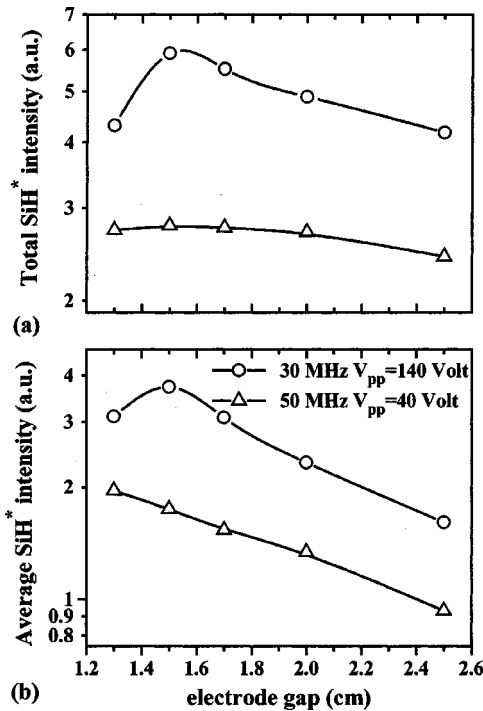


FIG. 6. (a) Total and (b) space averaged SiH ($\text{A}^2\Delta$) intensity as a function of the interelectrode gap at the frequencies of 30 and 50 MHz.

Furthermore, Figs. 6(a) and 6(b) show the total and the spatial average emission intensities, respectively, as a function of the electrode gap for frequencies of 30 and 50 MHz. The total emission intensity has been calculated by integrating in space the emission profiles presented in Figs. 5(a) and 5(b). For the 50 MHz case, the increase of the electrode gap has an effect on the total and the average emission intensities that is similar to its effect on the total discharge power and the power per discharge volume as shown in Figs. 1(a) and 1(b), respectively. Namely, the increase of the electrode gap slightly affects the total production of radicals, while it leads to a drop of the spatial average emission intensity. On the other hand, at 30 MHz the relation between the emission intensity and the power consumption is more complicated. The total emission intensity presents a maximum located at 1.5 cm, in contrast to the total power dissipation that has been found to increase with the electrode gap. This observation gives further support to the rationale presented in Sec. III A that attributes the increase of the total power at 13.56 and 30 MHz to the enhancement of the low energy electron-molecule collisions in the bulk plasma. As for the spatial average emission intensity, the existence of the maximum at 1.5 cm is maintained while the increase of the interelectrode space ($d > 1.5$ cm) results in a drop of the average intensity, which is similar to an equivalent decrease in the 50 MHz case.

Furthermore, the fact that the discharge efficiency in producing radicals varies with the interelectrode space also affects the film growth rate. This is shown in Fig. 7, which presents the deposition rate as a function of the electrode gap for 30 and 50 MHz. The measured deposition rates are quite

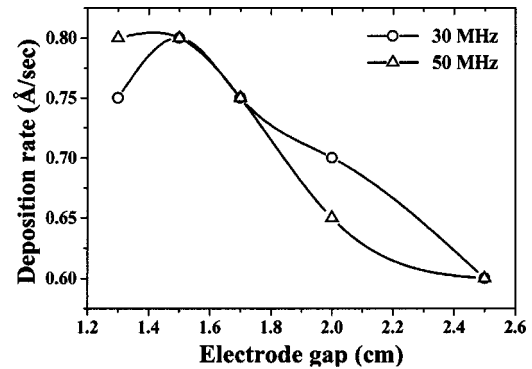


FIG. 7. Variation of the deposition rate as a function of the interelectrode gap for the 30 and 50 MHz discharges. The conditions are 0.5 Torr 2% SiH_4 in H_2 and constant rf voltage at each frequency.

low (< 1 $\text{\AA}/\text{s}$) under the present experimental conditions, leading to the deposition of microcrystalline silicon with high crystalline volume fraction.^{2,36} In the 30 MHz case there is a maximum in the deposition rate at 1.5 cm. The deposition rate at the lower gap used in the present study (1.3 cm) is higher for 50 MHz compared to 30 MHz, whereas the situation is reversed when the interelectrode gap increases ($d > 1.7$ cm). This observation indicates that when studying the effect of frequency on the deposition rate,^{9,23,37} one should always take into account the interelectrode gap used.

Understanding the dependence of the $\mu\text{c-Si:H}$ deposition rate on the electrode gap and of the different behavior at each frequency requires a closer look at the production of the radicals and on their spatial distribution in the discharge. The film precursors are neutral radicals that after being produced through silane dissociation can react in the gas phase or diffuse toward surfaces where they can participate in the surface reactions leading partially to the film growth. Previous work of this group^{38,39} has revealed that the composition of the flux of precursors depends mainly on the fraction of SiH_4 in the gas mixture as well as on the total gas pressure. Namely, in discharge conditions leading to relatively high deposition rates (high pressure, low dilution of SiH_4 in H_2), higher radicals as silicon dimmers (Si_2H_4 , Si_2H_5) determine the film growth. On the other hand, in discharge conditions that lead to lower growth rates and higher crystalline volume fractions (high dilution of SiH_4 in H_2 and low total gas pressure), the secondary gas phase reactions of radicals with SiH_4 are of minor importance. Consequently, the production of higher species and their contribution to the film growth is minor while silylene (SiH_2) and silyl (SiH_3) radicals determine the film growth. In addition, the role of ions and of the highly reactive ions in the gas phase silicon hydrides (Si , SiH) can be neglected, as their flux toward the surfaces is very low.³⁹ Thus in the present experimental conditions, the discussion concerning the effect of interelectrode space on the deposition rate can be focused on the gas phase and the surface reactivity of the SiH_3 and SiH_2 radicals.

Silyl (SiH_3) radicals have very low gas phase reactivity and wherever they are produced in the discharge have the chance to reach the surfaces and contribute to the film

growth. Thus, the flux of this radical to the surface is not hindered by the increase of the interelectrode space. Furthermore, considering the rather low film incorporation probability of this radical^{40,41} ($s \sim 0.1$) one can conclude that this radical cannot be responsible for the observed variation of the deposition rate with the electrode gap at both frequencies.

The case of silylene (SiH_2) is more complicated and the reaction of this radical with H_2 is rather slow⁴² ($5 \times 10^{-14} \text{ cm}^3/\text{s}$) while the reaction with SiH_4 competes with diffusion toward the surfaces (SiH_2 diffusion length, $\Lambda_{\text{SiH}_2} = 0.5 \text{ cm}$). Therefore, the contribution of this radical to the deposition rate will be strongly affected by the variation of the interelectrode space.^{13,14} Taking into account that this radical has a high incorporation probability,^{43,44} (0.65–0.8), the enhancement of its contribution to the film growth can lead to the observed variations of the deposition rate with the electrode gap (Fig. 7).

It is also worth noting that at 30 MHz the optimum of the deposition rate is achieved when the distance between the maximum rate of radical production and the surface approaches the diffusion length of SiH_2 . In the case of the optimum electrode gap, this distance can be estimated by using the spatial profiles of silane dissociative excitation [Fig. 5(a)] to 0.8 cm. The use of the emission profiles instead of the profiles of silane dissociation rate toward neutral radicals can produce a limited uncertainty in this calculation. However, in the present experimental conditions the total pressure is high enough to minimize the differences in the spatial distributions of these processes.⁴⁴ The fact that the distance is higher than the diffusion length of SiH_2 and that lower electrode gaps (1.3 cm) are not always followed by higher deposition rates indicates that the silane dissociation rate also plays an important role. The average production of excited radicals at 30 MHz [Fig. 6(a)] has been found to present an optimum at an intermediate electrode gap (1.5 cm). Thus assuming that this is also the case for the production of neutral radicals, the optimum of the deposition rate at 30 MHz is achieved through a better combination of the distance between the maximum rate of the radical production from the surface and the silane dissociation rate.

In the 50 MHz case, the continuous drop of the deposition rate with the increase of the interelectrode space is due to the displacement of the surface far from the maximum of radical production. Additionally at this frequency, the rate of the radical production is not expected to present an optimum but it will be enhanced by a decrease of the electrode gap. This is estimated to be the reason for the corresponding absence of an optimum of the deposition rate at intermediate electrode gaps. This estimation is partly supported by the dependence of the spatial average excited radical production on the electrode gap variation [Fig. 6(b)].

The absence of a maximum at either the deposition rate or the radical production for the specific range of interelectrode spaces is related to the fact that at 50 MHz, even at the lower electrode gap of 1.3 cm, the discharge is restricted between the two electrodes. This is because the sheath length of the

powered electrode remains less than the half of the total discharge length. However, a further decrease of the electrode gap ($< 1.3 \text{ cm}$) is expected to lead to a behavior similar to that of 30 MHz.

IV. CONCLUSIONS

A study of the effect of electrode gap on the properties of different driving frequency (13.56–50 MHz) SiH_4/H_2 discharges has been performed, aiming at the optimal deposition rate conditions of $\mu\text{c-Si:H}$ thin films.

The increase of the electrode gap under constant applied voltage and for low frequencies (13.56 and 30 MHz) leads to an increase of the total power consumption in the discharge due to an increase of the power dissipation in the expanded bulk. On the other hand, the average rate of energy coupling in the discharge drops, mainly due to the enhancement of the less effective bulk ohmic heating mechanism relative to the sheath collisional heating mode. At a higher frequency, the electrical properties remain unaffected by the variations of the electrode gap and this is related to the lower applied voltage and the less pronounced contact of the discharge with the reactor walls.

In the lower frequency case, the production of excited radicals presents a rather complex dependence on the variation of the electrode gap, presenting an optimum on intermediate interelectrode distances without following the trend of either the total or the average power dissipation. Dissimilarly, at 50 MHz the effect of electrode gap on the production of excited radicals coincides with the influence on power dissipation, i.e., the total radical production remains almost unaffected while the average rate of production drops with the electrode gap.

In addition, the effect of the interelectrode distance on the deposition rate has been found to be different for the two frequencies. In the case of 30 MHz an optimum rate exists at rather low electrode gaps, while for 50 MHz the deposition rate increases with frequency. In both cases, this behavior is related to the conditions ensuring a strong contribution of the highly sticking SiH_2 radicals to the film growth and a rather high silane dissociation rate.

Finally, the present study has revealed that the basic advantages that often lead to the use of frequencies higher than 13.56 MHz (use of lower applied voltage, higher radical production, higher deposition rate) also depend strongly on the choice of the electrode gap.

¹G. Bruno, P. Capezzuto, and A. Madan, *Plasma Deposition of Amorphous Silicon-Based Materials* (Academic, San Diego, CA, 1995).

²R. Schroop and M. Zeman, *Amorphous and Microcrystalline Silicon Solar Cells* (Kluwer Academic, Dordrecht, 1998).

³H. Curtins, N. Wyrsh, M. Favre, and A. V. Shah, *Plasma Chem. Plasma Process.* **7**, 267 (1987).

⁴F. Finger, U. Kroll, V. Viret, A. Shah, W. Beyer, X.-M. Tang, J. Weber, A. Howling, and Ch. Hollenstein, *J. Appl. Phys.* **71**, 5665 (1992).

⁵T. Kitajima, Y. Takeo, N. Nakano, and T. Makabe, *J. Appl. Phys.* **84**, 5928 (1998).

⁶M. Surenda and D. B. Graves, *Appl. Phys. Lett.* **59**, 2091 (1991).

⁷M. Capitelli, C. Gorse, R. Winkler, and J. Wilhelm, *Plasma Chem. Plasma Process.* **8**, 399 (1988).

⁸E. Amanatides and D. Mataras, *J. Appl. Phys.* **89**, 1556 (2001).

- ⁹L. Sansonnens, A. A. Howling, and Ch. Hollenstein, *Plasma Sources Sci. Technol.* **7**, 115 (1998).
- ¹⁰V. A. Godyak, R. B. Piejak, and B. M. Alexandrovich, *Plasma Sources Sci. Technol.* **1**, 36 (1992).
- ¹¹T. Kimura, K. Kaga, and K. Ohe, *Jpn. J. Appl. Phys., Part 1* **39**, 1351 (2000).
- ¹²D. Mataras, S. Cavadias, and D. Rapakoulias, *J. Vac. Sci. Technol. A* **11**, 664 (1993).
- ¹³M. J. Kushner, *J. Appl. Phys.* **63**, 2532 (1988).
- ¹⁴P. Kounavis, D. Mataras, N. Spiliopoulos, E. Mytilineou, and D. Rapakoulias, *J. Appl. Phys.* **75**, 1599 (1994).
- ¹⁵S. Isihara, M. Kitagawa, T. Hirao, and K. Wasa, *J. Appl. Phys.* **62**, 485 (1987).
- ¹⁶Y. Maemura, H. Fujiyama, T. Takagi, R. Hayashi, W. Futako, M. Kondo, and A. Matsuda, *Thin Solid Films* **345**, 80 (1999).
- ¹⁷D. Das, S. Chattopadhyay, A. K. Barua, and R. Banerjee, *J. Appl. Phys.* **78**, 3193 (1995).
- ¹⁸M. Isomura, M. Kondo, and A. Matsuda, *Sol. Energy Mater. Sol. Cells* **66**, 375 (2001).
- ¹⁹N. Spiliopoulos, D. Mataras, and D. Rapakoulias, *J. Vac. Sci. Technol. A* **14**, 2757 (1996).
- ²⁰D. Mataras, S. Cavadias, and D. E. Rapakoulias, *J. Appl. Phys.* **66**, 119 (1989).
- ²¹S. Stamou, D. Mataras, and D. E. Rapakoulias, *Chem. Phys.* **218**, 57 (1997).
- ²²A. A. Howling, J. L. Dorier, Ch. Hollenstein, U. Kroll, and F. Finger, *J. Vac. Sci. Technol. A* **10**, 1080 (1992).
- ²³M. Heintze, R. Zedlitz, and G. H. Bauer, *J. Phys. D* **26**, 1781 (1993).
- ²⁴M. A. Sobolewski, *IEEE Trans. Plasma Sci.* **23**, 1006 (1995).
- ²⁵M. A. Lieberman, *J. Appl. Phys.* **65**, 4186 (1989).
- ²⁶N. Spiliopoulos, D. Mataras, and D. E. Rapakoulias, *Jpn. J. Appl. Phys., Part 1* **36**, 66 (1997).
- ²⁷N. Spiliopoulos, D. Mataras, and D. E. Rapakoulias, *J. Electrochem. Soc.* **144**, 639 (1997).
- ²⁸B. Chapman, *Glow Discharge Processes* (Wiley, New York, 1980).
- ²⁹M. A. Lieberman and V. A. Godyak, *IEEE Trans. Plasma Sci.* **26**, 955 (1998).
- ³⁰Z. Wang, A. J. Liechtenberg, and R. H. Cohen, *Plasma Sources Sci. Technol.* **8**, 151 (1999).
- ³¹M. Surenda and D. B. Graves, *IEEE Trans. Plasma Sci.* **19**, 144 (1991).
- ³²M. A. Liebermann, *IEEE Trans. Plasma Sci.* **17**, 338 (1989).
- ³³G. R. Misium, A. J. Lichtenberg, and M. A. Lieberman, *J. Vac. Sci. Technol. A* **7**, 1007 (1989).
- ³⁴M. Capitelli, C. Gorse, R. Winkler, and J. Wilhelm, *Plasma Chem. Plasma Process.* **8**, 399 (1988).
- ³⁵M. Yan, A. Bogaerts, R. Gijbels, and W. J. Goedheer, *J. Appl. Phys.* **87**, 3628 (2000).
- ³⁶A. Matsuda, *J. Non-Cryst. Solids* **59&60**, 767 (1983).
- ³⁷E. Amanatides, D. Mataras, and D. E. Rapakoulias, *J. Appl. Phys.* **90**, 5799 (2001).
- ³⁸E. Amanatides, D. Mataras, and D. E. Rapakoulias, *Thin Solid Films* **383**, 15 (2001).
- ³⁹E. Amanatides, S. Stamou, and D. Mataras, *J. Appl. Phys.* **90**, 5786 (2001).
- ⁴⁰J. Perrin, M. Shiratani, P. Kae-Nune, H. Videtot, J. Jolly, and J. Guillon, *J. Vac. Sci. Technol. A* **16**, 278 (1998).
- ⁴¹A. Matsuda and T. Goto, *Mater. Res. Soc. Symp. Proc.* **164**, 3 (1990).
- ⁴²J. Perrin, O. Leroy, and M. C. Bordage, *Contrib. Plasma Phys.* **36**, 3 (1996).
- ⁴³M. Hertl and J. Jolly, *J. Phys. D* **33**, 381 (2000).
- ⁴⁴S. Stamou, E. Amanatides, D. Mataras, and D. E. Rapakoulias, 2nd World Conference on Photovoltaic Solar Energy Conversion, Vienna, 1998, p. 861.